Title

Treatment with JQ1, a BET bromodomain inhibitor, is selectively detrimental to R6/2 Huntington's disease mice

Journal

Human Molecular Genetics, 29(2)

ISSN

0964-6906

Authors

Kedaigle, Amanda J

Reidling, Jack C

Lim, Ryan G

et al.

Publication Date

2020-01-15

DOI

10.1093/hmg/ddz264

Peer reviewed

Human Molecular Genetics, 2020, Vol. 29, No. 2 202–215

doi: 10.1093/hmg/ddz264
Advance Access Publication Date: 7 November 2019
General Article

GENERAL ARTICLE

Treatment with JQ1, a BET bromodomain inhibitor, is selectively detrimental to R6/2 Huntington's disease mice

Amanda J. Kedaigle[1,†,‡], Jack C. Reidling[3,‡], Ryan G. Lim[3,‡,‡], Miriam Adam[2], Jie Wu[3], Brook Wassie[2], Jennifer T. Stocksdale[3], Malcolm S. Casale[3], Ernest Fraenkel[1,2,§] and Leslie M. Thompson[3,4,§,*]

[1]Computational and Systems Biology Program, [2]Department of Biological Engineering, Massachusetts Institute of Technology, Cambridge, MA 02142, USA, [3]Memory Impairment and Neurological Disorders Research Unit, and [4]Departments of Psychiatry and Human Behavior and Neurobiology and Behavior, University of California Irvine, Irvine, CA 92697, USA

*To whom correspondence should be addressed at: 4060 Gross Hall, 845 Health Sciences Road, University of California Irvine, Irvine, CA 92697-1705, USA. Tel: (949-824-6756); Email: lmthomps@uci.edu

Abstract

Transcriptional and epigenetic alterations occur early in Huntington's disease (HD), and treatment with epigenetic modulators is beneficial in several HD animal models. The drug JQ1, which inhibits histone acetyl-lysine reader bromodomains, has shown promise for multiple cancers and neurodegenerative disease. We tested whether JQ1 could improve behavioral phenotypes in the R6/2 mouse model of HD and modulate HD-associated changes in transcription and epigenomics. R6/2 and non-transgenic (NT) mice were treated with JQ1 daily from 5 to 11 weeks of age and behavioral phenotypes evaluated over this period. Following the trial, cortex and striatum were isolated and subjected to mRNA-seq and ChIP-seq for the histone marks H3K4me3 and H3K27ac. Initially, JQ1 enhanced motor performance in NT mice. In R6/2 mice, however, JQ1 had no effect on rotarod or grip strength but exacerbated weight loss and worsened performance on the pole test. JQ1-induced gene expression changes in NT mice were distinct from those in R6/2 and primarily involved protein translation and bioenergetics pathways. Dysregulation of HD-related pathways in striatum was exacerbated by JQ1 in R6/2 mice, but not in NTs, and JQ1 caused a corresponding increase in the formation of a mutant huntingtin protein-dependent high molecular weight species associated with pathogenesis. This study suggests that drugs predicted to be beneficial based on their mode of action and effects in wild-type or in other neurodegenerative disease models may have an altered impact in the HD context. These observations have important implications in the development of epigenetic modulators as therapies for HD.

[†]Amanda J. Kedaigle, http://orcid.org/0000-0001-6156-5046
[‡]Ryan G. Lim, http://orcid.org/0000-0001-6388-5158
[‡]The authors wish it to be known that, in their opinion, the first three authors should be regarded as joint First Authors.
[§]These authors are co-senior authors.
Received: July 11, 2019. **Revised:** September 20, 2019. **Accepted:** October 23, 2019

Introduction

Huntington's disease (HD) is an autosomal dominant neurodegenerative disease caused by an expanded CAG repeat within the *Huntingtin* (Htt) gene (1). The mutation encodes an expanded polyglutamine (Q) repeat tract within the corresponding Huntingtin (HTT) protein that causes adult onset disease when in the range of 40–60 repeats and juvenile onset HD with highly expanded repeats. Progressive neurodegeneration is observed primarily in the striatum together with atrophy of the cortex (2). Progressive and reproducible transcriptional dysregulation in the brain is strongly implicated as an important molecular phenotype in HD (3). Modifications of the epigenome may drive these transcriptional changes and represent a potential primary target for disease modification (3–7). Prior results with histone deacetylase inhibitors such as SAHA and sodium butyrate as well as reduction of the lysine-specific demethylase *JARID1c* demonstrated that modulating epigenetic enzymes can be beneficial in HD models (7–9). JQ1 is an epigenetic modulator that competitively binds the bromodomain and extra-terminal domain (BET) protein family and displaces these acetyl-lysine readers from chromatin, resulting in suppression of signaling events downstream of Pol II (10,11). JQ1 is one of a series of highly potent thienotriazolodiazepines that regulate bromodomain containing proteins and are in trials as therapeutics for cancer and other diseases (12–14). In addition, JQ1 effectively crosses the blood brain barrier (15), reduces neuroinflammation in mouse models (16,17) and selectively represses genes with super-enhancers implicated in various cancers, including the MYC oncogene (18,19). Beyond therapeutic benefit for a number of cancers and conditions involving inflammation (20), JQ1 has shown therapeutic benefit in a series of preclinical neurological settings, including acute retinal ganglion cell death in mice induced by N-methyl-D-aspartic acid (NMDA) excitotoxicity (21) and neuroinflammation, Tau phosphorylation in the 3xTg model of Alzheimer's disease (AD) (16) as well as reducing LPS-induced activation of BV-2 microglial cells (22). Given these attributes, JQ1 appeared to be a compelling therapeutic candidate for HD.

Histone post-translational modification states are associated with regulation of gene expression. For instance, trimethylation of lysine 4 on histone 3 (H3K4me3) is found nearly universally on the transcription start sites of actively transcribed genes (23) and changes significantly in HD tissues (7,24). Acetylation of lysine 27 on histone 3 (H3K27ac) is found near promoters and enhancers of active genes (25,26), with differential occupancy in HD neurons (5). H3K27ac shows extensive co-localization with BRD4, a target of JQ1, near highly expressed genes, and JQ1 treatment reduces this association (19,27).

In this study, we used R6/2 mice, an established model of HD that expresses the first exon of mutant *Huntingtin (HTT)* as a transgene with repeat expansion in the juvenile onset range (~120-150CAGs) and displays robust behavioral changes, neuroinflammation and transcriptional changes (28). R6/2 mice were treated with JQ1 to test whether this epigenetic modifier could improve behavioral symptoms, potentially through reduction of neuroinflammatory pathways, and normalize aberrant gene expression and epigenetic marks. JQ1 enhanced behavioral performance in non-transgenic (NT) mice at an early treatment time point. However, JQ1 treatment of R6/2 mice did not ameliorate behavioral phenotypes tested. Rather, JQ1 exacerbated one behavioral outcome and caused the mice to lose weight. At the end of the behavior study, the mice were sacrificed and brain tissue collected to examine the genome-wide gene expression and epigenetic state of their cortical and striatal tissues.

Transcriptomic signatures were quantified by measuring mRNA levels through RNA-seq for both cortex and striatum of JQ1 and vehicle-treated R6/2 and NT mice. The epigenetic state was evaluated through ChIP-seq to identify the genomic locations of two histone marks: H3K4me3 and H3K27ac. R6/2 mice compared to NTs showed characteristic differential gene expression changes described previously (7). Significant changes in gene expression were associated with JQ1 treatment; however, these changes were not specific *overall* to genes altered in HD. However, pathway analysis demonstrated that gene expression changes for a subset of synaptic genes consistently dysregulated in R6/2 mice and in human HD, were exacerbated by JQ1 treatment. For instance, *Dopamine receptor 2* (*drd2*), *Adora2A*, *Arc* and *Proenkaphalin* (*penk*), which are key neuronal genes down-regulated in HD (4,7,29), were further down-regulated in striatum. In addition, *Adora2A* is predicted to be an important regulator of JQ1 effects. Equivalent numbers of HD-affected genes were either exacerbated or altered back to NT levels, indicating a lack of a singular epigenetic influence of the drug on HD signatures, but rather a complex association of JQ1 treatment, epigenetic modulation and transcriptional changes. Interestingly, the same pathways altered in R6/2 by JQ1 treatment were not altered in NTs. There was an up-regulation of electron transport complex and protein translation genes, particularly those encoding ribosomal proteins and in initiation of protein translation in the JQ1-treated NT mice. JQ1 treatment led to alterations in H3K4me3 and H3K27ac signals in cortex but had almost no effect in striatal samples. These results provide insight into pathways that ultimately may influence HD phenotypes in R6/2 mice and potentially in human HD. Further, this study highlights the importance of identifying the molecular signatures impacted by drug treatments in the context of the HD mutation for more informed preclinical development of therapeutics for HD.

Results

JQ1 treatment of HD modeled R6/2 and NT mice

Ten R6/2 and NT mice per group were given daily IP injections (50 mg/kg) of JQ1 or vehicle control (10% cyclodextrin) beginning at 5–11 weeks. Mice were tested in a battery of behavioral phenotype tests to examine the effects of treatments on general health and motor function, including rotarod, pole test, grip strength and clasping as described (30). Figure 1A depicts the timeline for the study and the order of the behavioral tasks performed in mice.

Subjective observations after the first injection of JQ1 in R6/2 mice indicated that they appeared lethargic, hunched and were not responsive to handling. The mice appeared normal the next day and this response did not occur again with subsequent injections until they were in the 10th week when they displayed these characteristics again. NT mice were hyperactive and difficult to handle for the first several weeks of JQ1 dosing. R6/2 HD mice displayed the expected impairment (32) in behavioral tasks compared to NT mice (significant at $P < 0.05$, data not shown), with no effect of JQ1 treatment on impaired clasping or grip strength. All vehicle-treated mice behaved in a manner consistent with their genotype.

JQ1-treated R6/2 and NT mice gained weight at a similar rate to vehicle-treated mice until day 16 when R6/2 had a statistically significant reduction in weight gain (Figure 1B) as expected for

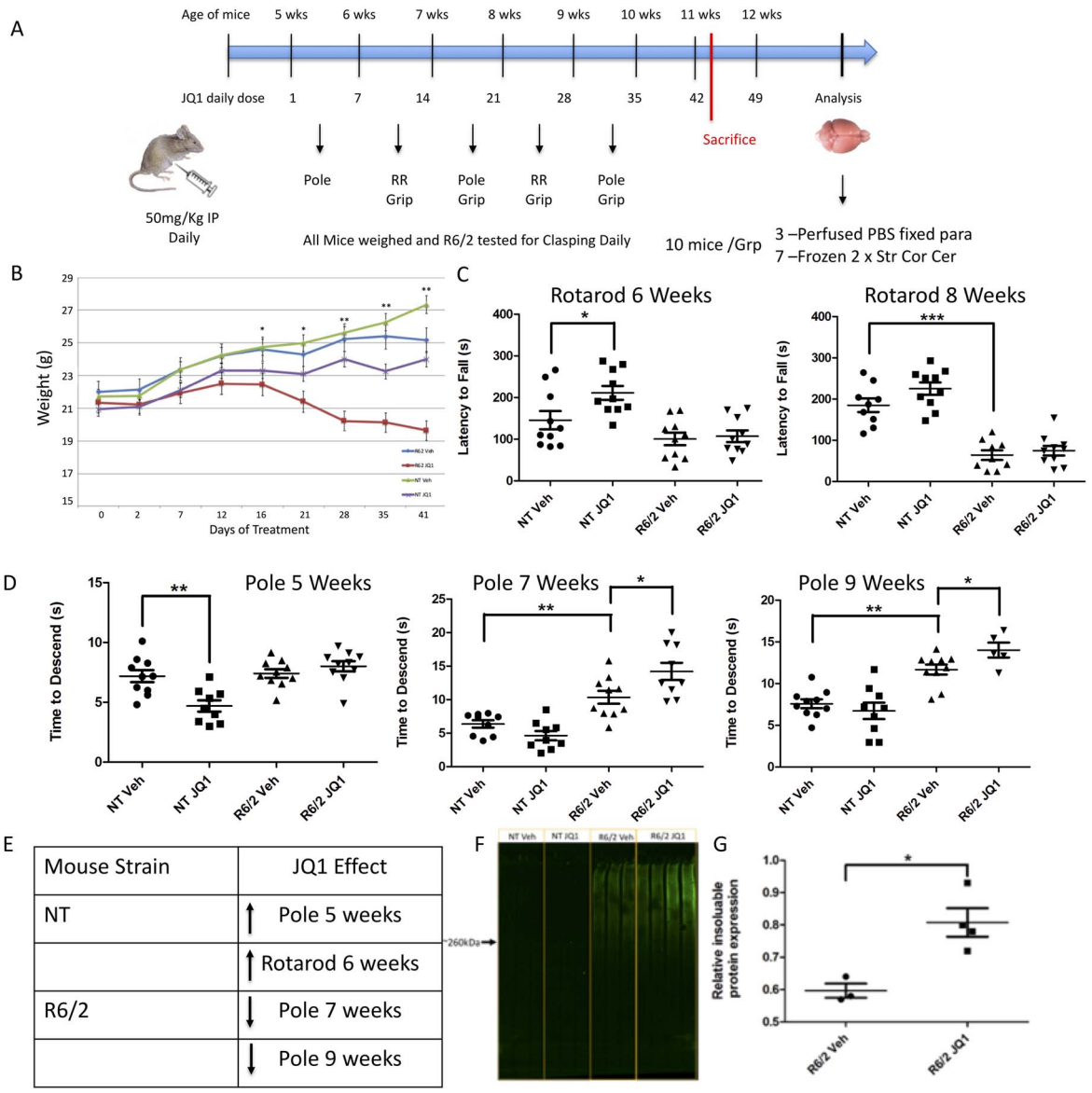

Mouse Strain	JQ1 Effect
NT	↑ Pole 5 weeks
	↑ Rotarod 6 weeks
R6/2	↓ Pole 7 weeks
	↓ Pole 9 weeks

Figure 1. Timeline and behavioral assessment of JQ1 treatment in R6/2 mice. (**A**) Timeline of JQ1 behavior study. (**B**) Weight of JQ1-treated mice. Mouse weight was recorded daily and graph displays average weights collected over time. (**C**) Outcome of rotarod test in JQ1-treated R6/2 mice. Rotarod indicates NT JQ1-treated mice have enhanced performance in the first trial. JQ1-treated R6/2 mice have no significant difference in performance compared to untreated mice in either the first or second trial. Genotype effect occurs in second trial comparing vehicle (Veh) treated NT to Veh treated R6/2. (**D**) Outcome of pole test in JQ1-treated R6/2 mice. Pole test indicates NT JQ1-treated mice descend faster in the first trial. JQ1-treated R6/2 mice have increased time to descend after second trial compared to vehicle treated R6/2 counterpart mice and the increased impairment continues in third trial. Genotype effect occurs in second and third trial comparing Veh treated NT to Veh treated R6/2. One-way ANOVA followed by Tukey's HSD test with Scheffé, Bonferroni and Holm multiple comparison calculation performed post hoc. $^{*}P < 0.05$, $^{**}P < 0.01$, $^{***}P < 0.001$ ($n = 10$). Graphs show means ± SEM. (**E**) Summary chart of behavior and weight. (**F**) JQ1 increases insoluble protein accumulation in R6/2 mice. Western blot analysis of striatal lysates separated into detergent-insoluble fractions detected using the LI-COR system. R6/2 mice show accumulated insoluble mHTT compared with NT. JQ1 treatment in R6/2 mice results in a significant increase of insoluble HMW accumulated HTT compared to Veh treated animals. (**G**) Graph indicating the quantitation of the relative protein expression for mHTT in R6/2 mice. Values represent means ± SEM. Statistical significance for relative insoluble accumulated mHTT protein expression in R6/2 was determined with a one-way ANOVA followed by Bonferroni post hoc test (R6/2: $n = 3$/veh, $n = 4$/JQ1) $^{*}P < 0.05$.

this model (28). By day 21, JQ1-treated R6/2 mice weight loss was exacerbated compared to vehicle treatment and the weight loss continued until the end of the study (Figure 1B). Subjective observations at the end of study indicated that R6/2 JQ1-treated mice were smaller, with scruffy coat, hunched posture and decreased activity compared to vehicle-treated R6/2 mice. In contrast, JQ1-treated NT mice did not appear different from vehicle-treated NT mice.

There was a significant difference between how R6/2 and NT mice responded to JQ1 treatment on two behavioral tasks: the pole test and the rotarod (Figure 1 C,D). JQ1 exacerbated the poor performance of treated R6/2 mice compared to vehicle-treated mice on the pole test. However, treatment enhanced performance on this task in NT mice compared to vehicle controls (Figure 1D). The exacerbated impairment of R6/2 mice (over genotype effects compared to NT) was observed in the second

pole test trial and persisted for the third trial (Figure 1D). The JQ1-mediated enhancement for NT mice occurred in the first trial but was not statistically significant in the other trials. Our results on the pole test do not exclude the possibility that JQ1 is impacting mouse anxiety and motivation to descend. However, the effect would be different for NT versus R6/2 mice as JQ1-treated NT mice descend faster (more anxiety and more motivation), while R6/2 mice descend slower (less anxiety and less motivation). JQ1 had no effect on the ability of R6/2 mice to perform on the rotarod; however, it did enhance the ability of NT mice to remain on the rotarod (Figure 1C). This rotarod improvement for NT mice occurred in the first trial but was not statistically significant in the second trial. A summary of the behavioral results is provided in Figure 1E.

JQ1 increases pathogenic accumulation of mHTT

We examined the impact of JQ1 treatment on a high molecular weight (HMW) mutant huntingtin (mHTT) species that accumulate in R6/2 mouse brain. Previous studies indicate that reduction of these insoluble proteins corresponds to improved behavioral outcomes in R6/2 mice (30,31). Accumulation of detergent-insoluble HTT was present in R6/2 striatum as expected (Figure 1F) and treatment with JQ1 increased this accumulation (Figures 1F,G), consistent with the worsening of HD phenotypes. HMW mHTT was not detected in NT mice. The smear in the image is a HMW species present in the detergent-insoluble fraction of R6/2 mice that only appears in the presence of mHTT. Detergent-insoluble fractions contain primarily nuclear proteins and HMW HTT species (likely multimers or potentially insoluble oligomers and fibrils) and accumulated forms of SUMO- and ubiquitin-modified proteins (32).

RNA-seq analysis of JQ1-treated mice shows no overall HD-specific pattern of changes

At the end of the behavioral study, we investigated whether transcriptomic signatures could inform the behavioral changes observed with JQ1 treatment. Tissue from four mice per group for cortex and three mice per group for striatum were selected and RNA from one hemisphere of cortex and one hemisphere of striatum each were analyzed by RNA-seq. After RNA isolation and QC, all samples were used for library prep using Illumina's Truseq polyA+ RNA library prep kit v2, along with ERCC ExFold spike-in, and sequencing was performed on all samples using the Hiseq2500 to obtain ~15M PE100 reads/sample. After mapping and count quantification, normalized count data were used for unsupervised exploratory analysis using principal component analysis (PCA) on the top 500 most variable gene expression profiles (Figure 2A). PCA of all 28 samples showed clear separation between cortical and striatal samples along PC1 with R6/2 and NT group separating on PC2 (Figure S1). However, cortical samples 10c (R6/2 vehicle treated) and 3c (NT vehicle treated) have gene expression profiles that dramatically deviate from the rest of the samples; therefore, they were removed from the RNA-seq differential expression analysis. In Figure 2B–E, the analyses showed clear separation between JQ1-treated and untreated samples per group in each brain region, except for the NT striatal sample, which did not show separation between the treated and untreated groups. In Figure 2A, variance along PC2 (18%) separates NT and R6/2 samples, indicating a genotype effect on transcriptional dysregulation for both cortical and striatal samples. As expected, differential expression analysis and GO enrichment analysis (33) of gene differences between vehicle R6/2 and NT mice for both striatal and cortical samples showed significant changes in terms related to neuronal development and function as previously described (4,7,29) (Supplementary Material, Figure S2 and Tables S1 and S2). The number of differentially expressed genes (DEGs) was much larger in the striatum then cortex (Figure 3, number of DEGs per protocol). JQ1 treatment resulted in DEGs for the following cases: In the cortex, 182 DEGs were identified in JQ1-treated R6/2 compared to vehicle-treated R6/2 mice, and 461 DEGs were differentially expressed between JQ1-treated NT and vehicle-treated NT mice. In the striatum, 1162 genes were differentially expressed in JQ1-treated R6/2 compared to vehicle-treated R6/2 mice, but only 16 genes were differentially expressed between JQ1-treated NT and vehicle-treated NT mice (Figure 3). Fewer genes are differentially expressed between vehicle-treated R6/2 and vehicle-treated NT mice (5561 genes) than are differentially expressed between JQ1-treated R6/2 and vehicle-treated NT mice (5921 genes) in the striatum. Interestingly, the same comparisons in the cortex showed the opposite pattern, with twice as many genes differentially expressed in the vehicle-treated R6/2 versus vehicle-treated NT mice compared to the corresponding comparison of JQ1-treated R6/2 versus vehicle-treated NT mice (Figure 3A). Figure 3B and C show scatter plots of log2FC for each of these comparisons. The striatal samples show some novel gene changes in the R6/2 JQ1-treated versus NT vehicle contrast (e.g. *Dnajc22*, *Transketolase Like 1, Tktl1*). In the cortical samples, the majority of the novel gene changes show a shift both up and down in the R6/2 JQ1-treated versus NT vehicle contrast compared to the R6/2 versus NT vehicle contrast, as well as exacerbation of gene changes found in the R6/2 versus NT vehicle contrast.

Next, we asked if the overall genes changed by the JQ1 treatment in R6/2 mice were related to those changed by expression of the mutant HTT exon1 transgene (hereafter designated as mHTT). We compared two sets of dysregulated genes: (1) genes that were dysregulated upon JQ1 treatment of R6/2 mice (the 'JQ1 effect') and (2) genes that were dysregulated in vehicle-treated R6/2 mice compared to NT mice (the 'mHTT effect'). No overall pattern was seen in either tissue type—the scatter plots are not significantly sloped in any direction—indicating that on the whole, HD-related genes were not selectively changed by JQ1 treatment (Figure 4). JQ1 treatment in R6/2 cortex affected expression of 178 genes, of which 59 were also altered in the comparison of untreated R6/2 versus NT animals (Figure 5A, top). While this overlap is statistically significant ($P < 3.22e\text{-}15$, Fisher's right tailed test), it represents a small fraction of the 3133 DEGs in cortex that are induced by mHTT expression in untreated animals (Figure 5A, bottom). In contrast, the treated striatal R6/2 sample had 1162 DEGs that overlapped with 703 DEGs found in the R6/2 versus NT striatum (Figure 5B, top). In our previous study (7), 949 DEGs were identified in the cortex of 12-week-old R6/2 mice compared to NT and 170 at 8 weeks. Of these, 643 genes were overlapping with the 3133 DEGs identified in this current study (Figure 5C top). A total of 5921 DEGs were identified in the striatum of R6/2 mice compared to NT in the current study (Figure 5B, bottom), while 580 were identified in our previous study at 12 weeks and 134 at 8 weeks (Figure 5C, bottom). A total of 482 genes overlap the previous study with our current study. We believe the increase in DEG number can be attributed to the increased depth of sequencing and updated methodology used for this study.

We determined if JQ1 treatment had a localized effect on specific cell types of the cortex and striatum using the Cell-type Specific Expression Analysis tool (34). In R6/2 cortex, the

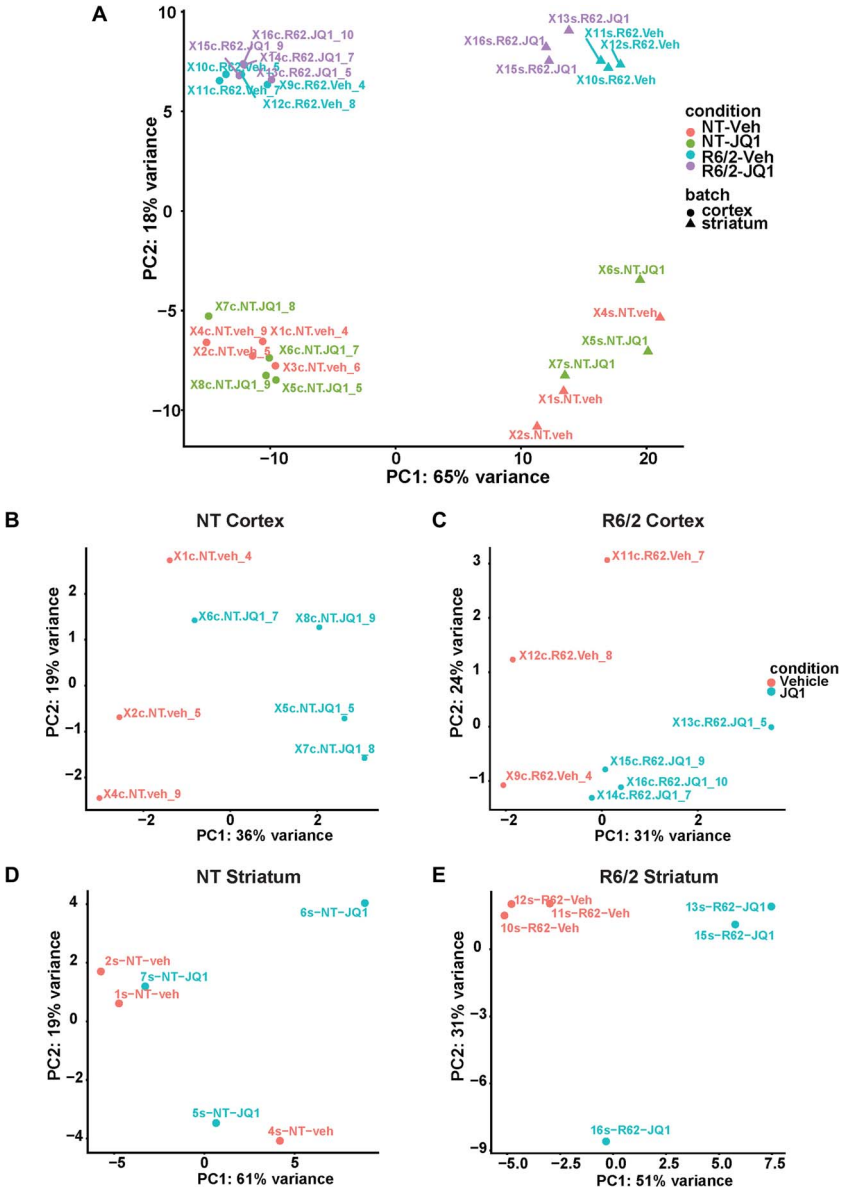

Figure 2. Exploratory analyses of JQ1-treated and untreated cortical and striatal samples. (**A**) PCA analysis of JQ1-treated and untreated R6/2 and NT mice in cortical and striatal samples. PCA clusters samples that are similar across all genes into groups. Maximal variance, along PC1 (65%) separates cortical and striatal samples, while PC2 (18%), separates NT and HD R6/2 samples indicating a robust genotype effect on transcriptional dysregulation. Additionally, a minor, but clear, separation can be seen within groups between JQ1-treated and untreated samples. (**B**) PCA of NT cortex samples. (**C**) PCA of R6/2 cortex samples. (**D**) PCA of NT Striatum samples. (**E**) PCA of R6/2 striatum samples. Each PCA shows clear separation along PC1 of the treated versus untreated samples, except for the NT striatum, which had no clear separation.

effects of JQ1 were most consistent with genes expressed in immune cells. In R6/2 striatum, by contrast, JQ1-responsive genes were more specific to neurons, including medium spiny neurons (Figure S3). To further assess the cell-type specific effects of JQ1 on NT and R6/2 cortex and striatum, we looked at the relative expression patterns of genes enriched in either neurons or astrocytes compared to all other cell types of the CNS (Table S3). The top 500 enriched genes for each cell type were generated using the cell-type expression enrichment tool by the Barres lab (https://web.stanford.edu/group/barres_lab/brain_rnaseq.html). FPKMs for these genes from our data were used for clustering (Figure 3D; Supplementary Material, S4A–C, Table S4–S7). Interestingly, JQ1 seemed to change the expression of neuronal genes mainly in cortex of the NT samples, causing a decrease in gene expression of some neuronal genes (Calb2, Ctxn2, Dlx6) while increasing expression of others (Drd2, Bcl11b, Neurod6). In contrast, JQ1 treatment of R6/2 primarily changed neuronal gene expression in the striatum with limited changes in the cortex. In the cortical samples the effect seemed limited to astrocytes, slightly increasing the level of genes that were decreased in the R6/2 versus NT comparison. In the striatum, JQ1 seemed to only impact neuronal genes, slightly enhancing the down-regulation of genes in the R6/2 versus NT contrast. However, JQ1 primarily increased the levels of neuronal genes that were both decreased and increased in the R6/2 samples compared to NT.

Expression levels and fold change were used to determine if JQ1 treatment 'restored' the expression back to NT levels, or if the treatment 'aggravated' the expression by exacerbating the levels even further away from NT levels. In the cortical samples, the 32

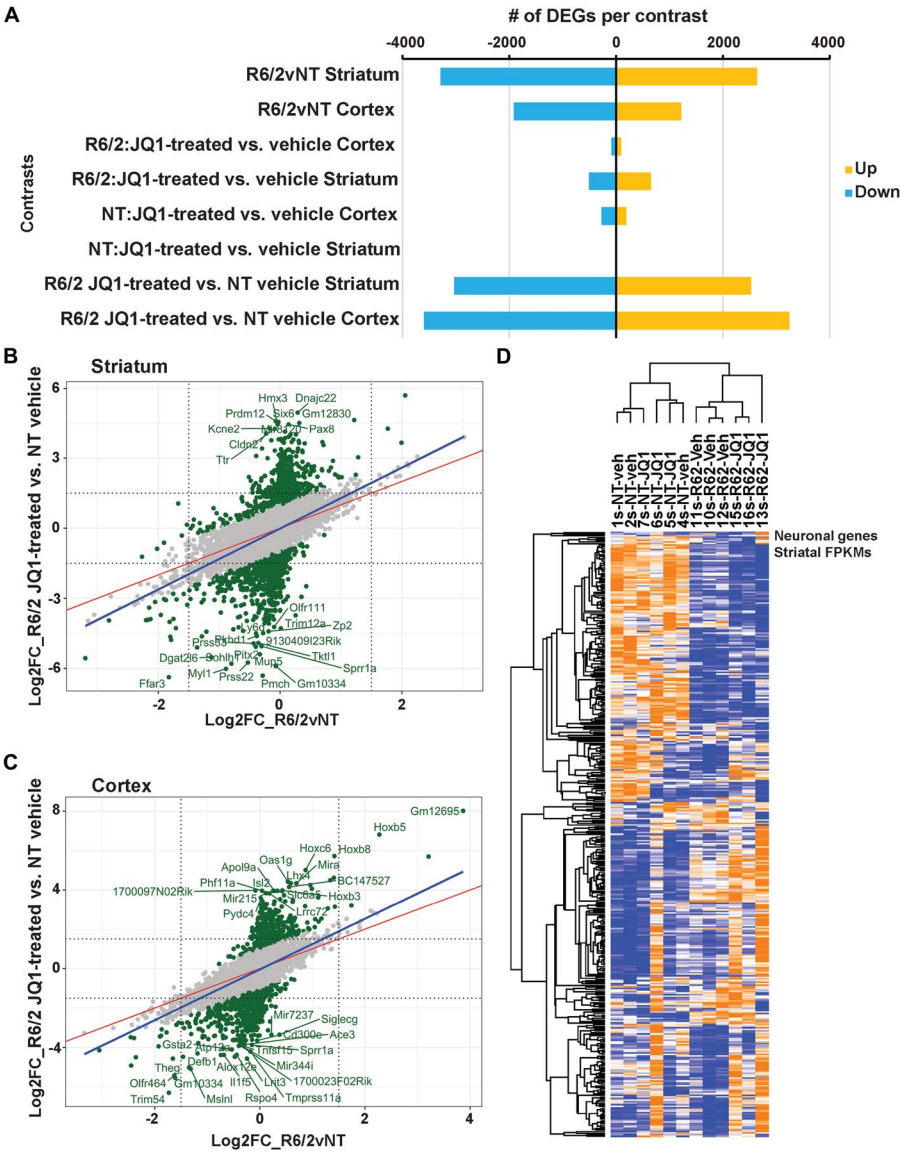

Figure 3. The effects of JQ1 by differential expression analysis and contrast comparisons. (**A**) Number of DEGs in each of the main comparisons of JQ1-treated and vehicle-treated animals. (**B** and **C**) Scatterplot of log2 Fold change comparing R6/2 versus NT and R6/2-JQ1 versus NT-vehicle contrasts in striatum and cortex, respectively. The green dots represent genes with |log2FC difference| > 1 between the two contrasts, while labeled genes represent the differences of >3.5. The red line marks perfect correlation with a slope of 1, and the blue line is a regression line based on linear model using log2FC values. (**D**) Spearman's hierarchical clustering of FPKM values from striatal samples for the top 500 neuronal enriched genes, over all other cell type in the CNS, row min–max are continuously colored from blue to orange.

genes that are further aggravated by JQ1 treatment are involved in calcium transport (Supplementary Material, Table S8). The 27 genes that are restored ('cured') by JQ1 were mainly extracellular matrix related genes.

In the striatum, of the 703 overlapping DEGs, 364 of these were found to be aggravated while an equivalent 338 were at least partially restored to NT levels (Figure 5B, bottom; Supplementary Material, Table S9). The majority of overlapping genes were all down-regulated in the R6/2 versus NT vehicle contrast. Therefore, genes that were restored were up-regulated by JQ1, and genes that were aggravated were further down-regulated. GO analysis of each group identified general terms such as biological regulation, signaling, localization and behavior in both categories (Figure 6). This analysis suggests that JQ1 did not have a selective effect on HD dysregulated genes.

Histone mark ChIP-seq analysis shows modest changes and selective HD-related restoration of two histone marks in cortex

Next, we investigated epigenetic changes caused by JQ1 treatment. We performed a ChIP-seq experiment on the cortex and striatum to find the genomic locations of the histone marks H3K4me3 and H3K27ac. In agreement with previous work (4,5,7), there were many changes to H3K4me3 and H3K27ac marks between R6/2 and NT mice in both tissues. However, JQ1 treatment caused surprisingly few significant changes in the two histone marks in the cortex (Supplementary Material, Table S10) and almost no changes in the striatum (Table 1).

We ran a similar analysis as we did for gene expression changes to look for HD-related patterns in the epigenetic

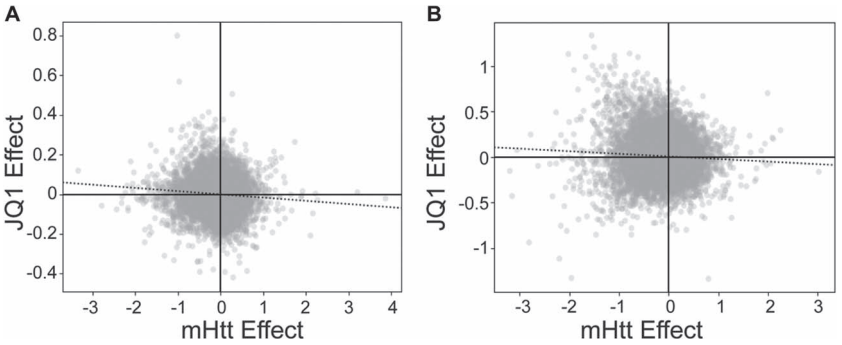

Figure 4. Scatter plot of logFC of RNA-seq reads. Genes graphed according to the log fold change of its mRNA between vehicle-treated R6/2 tissue and NT tissue ('mHtt effect') versus the log fold change between JQ1-treated and vehicle-treated R6/2 tissue ('JQ1 effect'), in cortex (**A**) and striatum (**B**). Best fit lines (dotted lines) indicate that there is no strong linear correlation of these changes, so genes that change in expression in HD are not generally the ones being changed by JQ1 treatment.

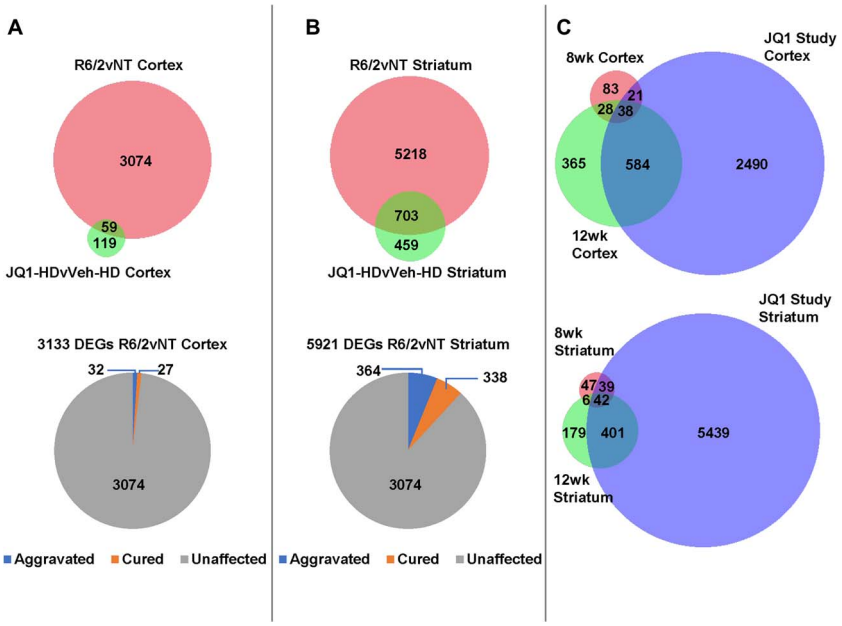

Figure 5. Overlap of genes changed by JQ1. (**A**) Venn diagram of number of DEGs in R6/2 versus NT cortex (red) and R6/2 JQ1-treated versus vehicle (green), and pie chart showing number of aggravated and cured genes in cortex. (**B**) Venn diagram of number of DEGs in R6/2 versus NT striatum (red) and R6/2 JQ1-treated versus vehicle (green), and pie chart showing number of aggravated and cured genes in striatum. (**C**) Venn diagram comparing old R6/2 DEGs against current study for cortex (upper) and striatum (lower).

Table 1. Few differential epigenetic peaks in the striatum caused by JQ1 treatment. For two histone marks, ChIP-seq results were compared to determine the effect of JQ1 in both R6/2 HD mice and in NTs and to determine the differences between R6/2 mice and NT mice when treated with vehicle control (veh). The number of peaks called as 'biased' to each sample by DiffBind and DESeq2 is shown

Histone mark	Treatment	Control	Peaks increased in treatment	Peaks increased in control
H3K4me3	JQ1 in R6/2	veh in R6/2	0	2
	JQ1 in NT	veh in NT	0	0
	veh in R6/2	veh in NT	568	715
H3K27ac	JQ1 in R6/2	veh in R6/2	9	5
	JQ1 in NT	veh in NT	0	0
	veh in R6/2	veh in NT	1871	2928

ChIP-seq data. In this case, we graphed the fold-change of counts per million reads around the transcription start sites (−2 kb, +3 kb) of genes in R6/2 versus NT vehicle-treated mice (the mHTT effect), compared to the same value for JQ1-treated R6/2 mice versus vehicle-treated R6/2 mice (the JQ1 effect). In the striatum, there was no overall pattern between these two changes (Figure 7), indicating that the genes that experience a change in histone mark levels with JQ1 treatment are not the same ones that experience a change in HD overall. In the cortex, where we had fewer ChIP-seq samples, there remains no significant slant for either histone mark, although the trend for both is a slight negative slant to this pattern (Figure S5). This indicates a trend in which JQ1 might partially reverse the epigenetic effects of mHTT in the cortex, but not in the striatum. Any

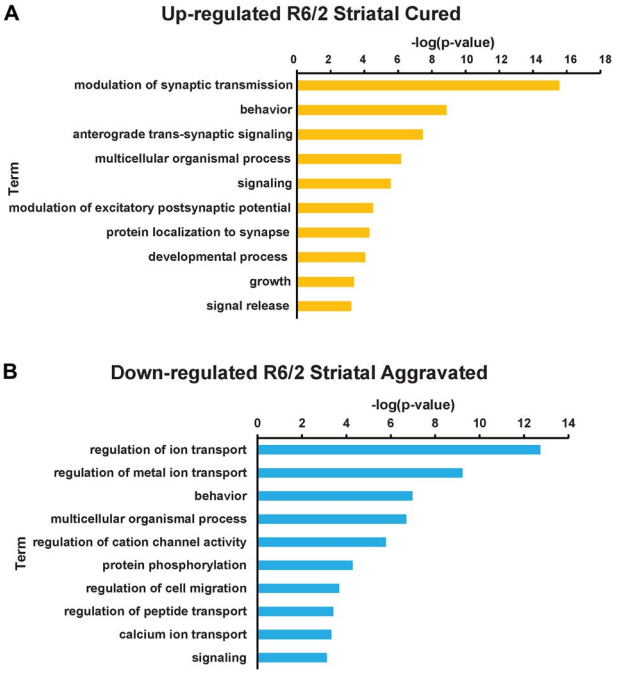

Figure 6. GO analysis of striatal samples. (**A**) GO biological process for genes that were up-regulated and 'cured' by JQ1 treatment. (**B**) GO cellular component for genes that were down-regulated and 'aggravated' by JQ1 treatment.

modest restoration of R6/2-induced changes in H3K4me3 was not carried through to gene expression or to phenotypic improvement.

The preceding analyses suggest that the epigenetic effects of JQ1 are not sufficiently specific for HD-affected genes to have a therapeutic effect. In previous work (5,7), we showed that genes that had a certain broad 'profile', or shape, of their H3K4me3 and H3K27ac reads extending from their transcription start site into the coding region were significantly enriched for genes that became transcriptionally dysregulated in HD cells. We therefore asked if there was a profile associated with genes that changed expression upon treatment with JQ1. Genes that change in expression upon JQ1 treatment did not have any consistent profile for either H3K4me3 or H3K27ac in the cortex (Figure S6). However, genes that had a broad profile extending into the coding region for both H3K27ac and H3K4me3 were indeed enriched for genes dysregulated by JQ1 in the R6/2 cortex (Figure S7). We also tested whether genes associated with super-enhancers, which are generally related to genes with the broad profile in these histone marks, are associated with genes dysregulated by JQ1, and found a significant association with down-regulated genes in the striatum (Supplementary Material, Figures S6C and S7C) Therefore, genes marked by a specific epigenetic profile, which are vulnerable to transcriptional dysregulation in HD, are targeted by JQ1 treatment in the striatum, but not the cortex. This shared targeting of an epigenetic profile, however, was not sufficient to produce coordinated RNA-seq changes in either region (Figure 4).

JQ1 differentially affects NT mice showing up-regulation of bioenergetic pathways and protein translation

JQ1-treated NT mice showed enhanced performance in the first pole and rotarod behavior tests. Therefore, we investigated pathways impacted in these mice. A striking finding from pathway analysis (GO and QIAGEN's Ingenuity Pathway Analysis (IPA) (35)) of NT cortex DEGs (Supplementary Material, Table S11), is the significant up-regulation of protein translation components and electron transport chain (ETC) encoding genes. GO analysis revealed an enrichment in up-regulated genes involved in several aspects of protein translation and metabolic processes and down-regulated genes involved in neuronal development and synaptic function, while IPA analysis shows predicted activation of EI2F signaling (Figure 8A & B). In addition to translation, the ETC was also enriched, showing an up-regulation of genes in complex I, III, IV and V (Figure 8C and D).

HD associated pathways are selectively dysregulated in R6/2 following JQ1 treatment

Several pathways relevant to disease pathogenesis were further dysregulated by the drug in R6/2 mice but not in NTs. DEG lists from R6/2 cortex upon JQ1 treatment (Supplementary Material, Table S12) were mined for networks, pathways and functional

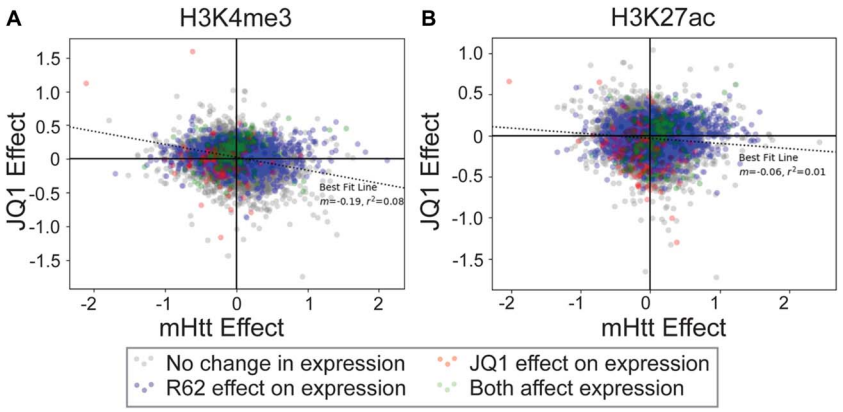

Figure 7. Scatter plot of logFC of ChIP-seq reads in mouse striatum. ChIP-seq reads from H3K4me3 (**A**) and H3K27ac (**B**) were counted in the area 2 kb upstream through 3 kb downstream from each transcription start site in striatum. Read counts were normalized to counts per million, and averaged over three replicates per condition. Genes are plotted according to the log fold change between vehicle-treated R6/2 tissue and NT tissue ('mHtt effect') versus the log fold change between JQ1-treated and vehicle-treated R6/2 tissue ('JQ1 effect'). Each gene is colored according to whether they changed in mRNA expression in either comparison (uncorrected $P < 0.01$). Best fit lines (dotted lines) indicate there is no significant linear trend. Genes that change in expression do not appear to cluster to any one part of the distributions, but are scattered throughout.

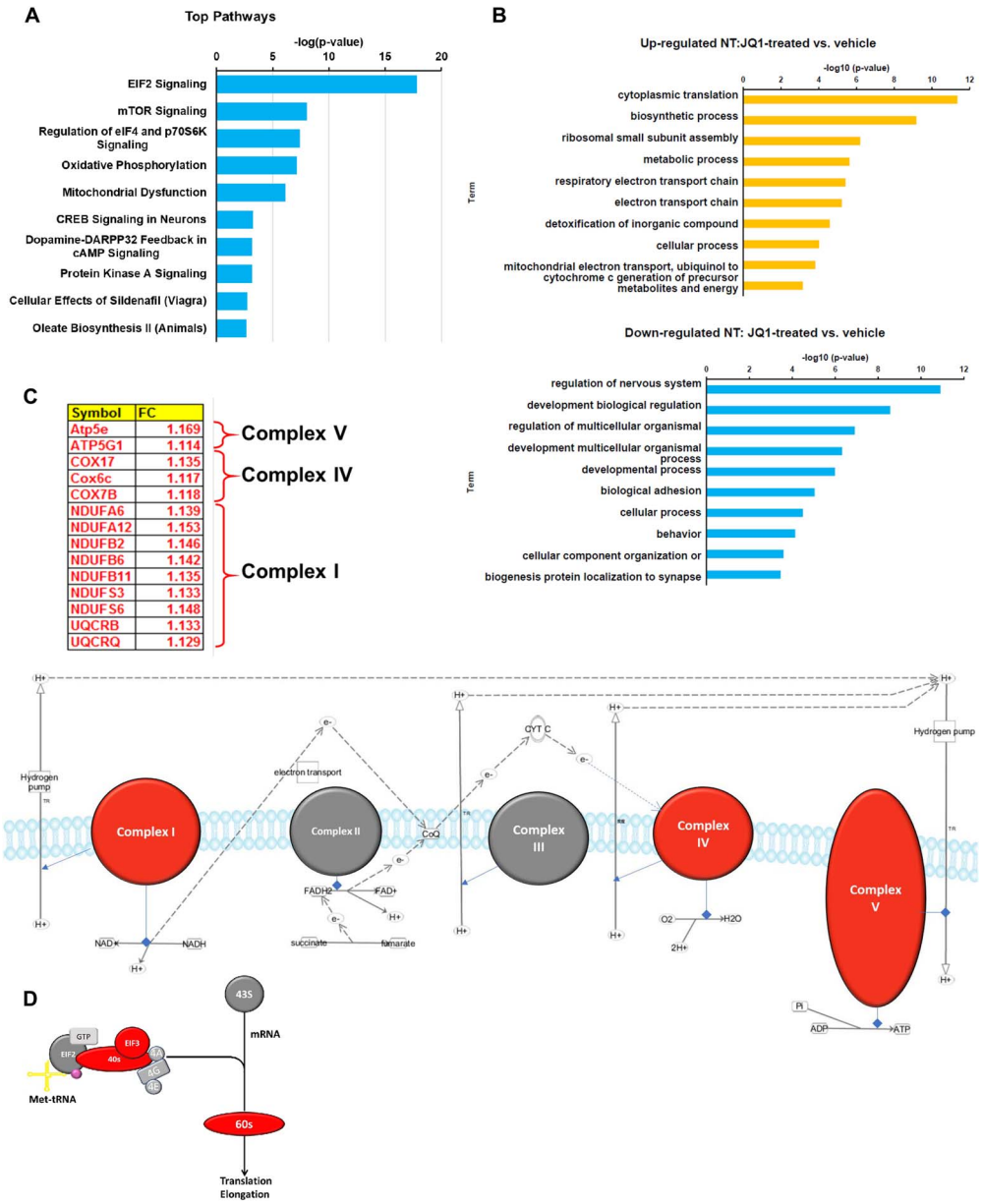

Figure 8. Analysis of JQ1 treatment in cortex NT mice. (**A**) Pathway analysis of genes dysregulated by JQ1 treatment in NT mice cortex. (**B**) GO analysis of JQ1-treated NT cortex. (**C**) Genes up-regulated in ETC pathway. (**D**) Genes up-regulated in the EIF2 signaling pathway.

categories using IPA and GO analysis. In cortex, GO analysis of up-regulated genes in the R6/2 cortex after JQ1 treatment show enrichment for genes involved in apoptosis and other cellular responses to pathogens and down-regulated genes involved in ion homeostasis as the main biological processes affected (Figure 9A). IPA network analysis suggests that *Adora2a* could be a driver regulating many of the genes that become dysregulated in the R6/2 cortex after JQ1 treatment and that its function is further inhibited after JQ1 treatment (Figure 9B). Inflammatory responses also appear to represent hubs with predicted activation of NFkB complex and NFKBIA. CREB and BDNF also are represented as regulatory hubs. There were only 16 DEGs for JQ1-treated NT striata, therefore no pathway enrichment was observed.

In R6/2 striatum, many HD-specific neuronal pathways were further dysregulated by JQ1 (Supplementary Material, Table S13). Pathway and GO analysis of JQ1-treated R6/2 striatum showed pathways and terms related to neuronal function and relevant to HD pathology (Figure 10A and B). For instance, there is an overrepresentation of G-protein coupled receptors, axonal guidance, cell adhesion and cytoskeleton (Figure 10A–C). We have previously observed these pathways and processes to be dysregulated in HD mouse tissue and differentiated HD-iPSCs (7,36). An overrepresentation of CAMK receptors is seen, with exacerbation of *CamK2B* down-regulation (Figure 10C). A significant dysregulation of GABA receptor signaling is also observed (Figure 10D). These include exacerbation of HD-associated transcriptional changes defined in multiple systems, including human brain (29). For instance, there are alterations in cAMP-mediated signaling, including further down-regulation of *Drd2*, *Drd1A* and *Adora2A* (Figures 9B, 10C and D; Supplementary Material, Table S13) as well as *Arc*, *CamKV* and *Penk*. Finally,

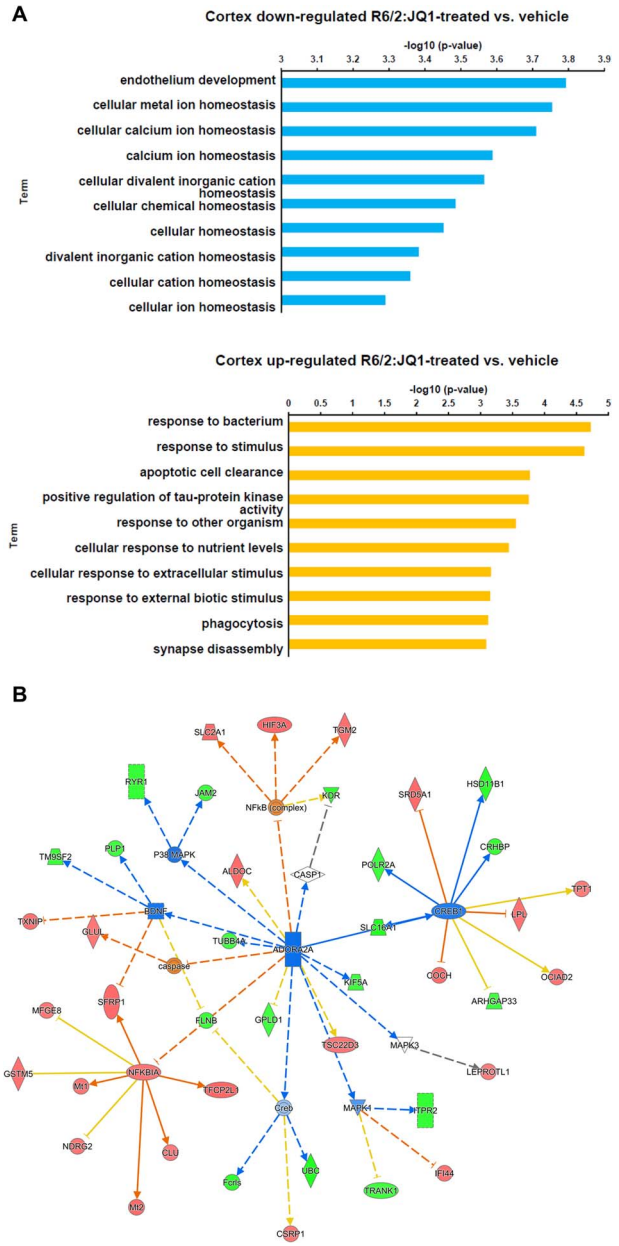

Figure 9. GO and network analysis of genes dysregulated by JQ1 treatment in cortex of R6/2 mice. (**A**) GO analysis of JQ1-treated R6/2 cortex. (**B**) IPA network analysis showing *Adora2a* as potential causal driver of gene expression differences in JQ1-treated R6/2 cortex.

dysregulation of ubiquitin and deubiquitinating enzymes are identified including down-regulation of deubiquitinating protein genes *Usp2* and *Usp28* and up-regulation of *Usp29*, *Usp46* and *Usp51* (data not shown).

Taken together, these data suggest that the context of JQ1 administration, e.g. in the presence of mHTT exon 1 protein expression, may directly impact the behavioral and molecular outcomes.

Discussion

Despite the promising performance of JQ1 in pre-clinical trials for certain diseases, JQ1 treatment of R6/2 mice did not improve phenotypes. The R6/2 mice did not tolerate the drug well, as prolonged treatment caused them to lose weight, become lethargic and hunched (typical signs of distress) and showed exacerbation of a behavioral task typically impaired in these mice. Several studies in wild-type mice have shown that this same dose of JQ1 was well-tolerated (10,11,37), and indeed the NT mice in this study tolerated the drug well, continued to gain weight and had enhanced performance on the pole and rotarod tests. Therefore, the impact of JQ1 is different in the context of HD. The R6/2 HD mice thus appear to be vulnerable to the drug in a way that wild-type mice are not and do not benefit from its effects.

Comparing genes that were dysregulated in R6/2 versus NT mice to the genes that were dysregulated in R6/2 upon JQ1 treatment, as well as focusing explicitly on those genes that were recovered or worsened, showed that overall there was not a clear pattern of restoration or exacerbation in HD gene expression changes. In the cortex, there was a non-significant trend toward restoration of H3K4me3 and H3K27ac levels. This is significant as H3K27ac, extensively present within gene bodies of genes with super-enhancers (4), co-localizes with BRD4, the latter displaced by JQ1 treatment (38). This trend of recovery toward NT-like patterns of histone marks near genes with altered expression in R6/2 was only present in the cortex, not the striatum.

There were surprisingly few changes to histone mark peaks after JQ1 treatment that reached statistical significance in the ChIP-seq studies. Although JQ1 inhibits proteins involved with the detection of histone acetylation, it appears to have minor changes on the underlying histone marks themselves. Other studies in cancer cell lines (39,40), mouse fibroblasts (41) and human osteoblasts (42) also found only modest changes in histone marks after JQ1 treatment, and suggested that while BRD4 occupancy of those regions are changed by the drug, the underlying epigenetic states are not.

BET proteins have recently been implicated as master regulators of global transcription elongation (18,38). BRD4 facilitates release of promoter-proximally paused RNA polymerase II (PolII) and transcription elongation. Binding of JQ1, however, preferentially releases BRD4 from chromatin massive enhancer elements, e.g. super-enhancers, resulting in reduced pause release and reduced transcription of select genes containing super-enhancers. Intriguingly, striatal super-enhancers have been described to drive transcription of genes characterized by low levels of paused RNA Pol II (4) and neuronal genes that are preferentially down-regulated in the R6/1 and R6/2 HD mouse striatum are characterized by decreased RNA Pol II in gene bodies at promoters having a broad H3K27ac profile and subsequently increased RNA Pol II pausing (4). This suggests a contribution of RNA Pol II pausing in mis-regulation of super-enhancer containing neuronal function genes that represent an HD epigenetic signature. These genes significantly overlap with striatal neuronal pathway genes that have exacerbated down-regulation by JQ1 treatment in R6/2 mice, including *Drd2*, *Pde10A*, *Adora2A*, *Arc* and others suggesting that in the context of mHTT, JQ1 displacement of BRD4 may preferentially exacerbate the down-regulation of critical striatal genes, resulting in worsening HD phenotypes in R6/2 mice (Supplementary Material, Tables S12 and S13, Figure S7).

Recently, a study of the effects of JQ1 in the brain of wild-type mice found that JQ1 treatment blocks memory in mice by affecting synaptic-activity-induced transcription, including blockage of BDNF-induced increases in immediate early genes such as *Arc*, *Fos* and *Nr4a1* (37), each of which are dysregulated in untreated R6/2 mice and further dysregulated in JQ1-treated R6/2 striatal tissue. These changes may also result through the selective effects of BRD4 displacement. JQ1 treatment was also

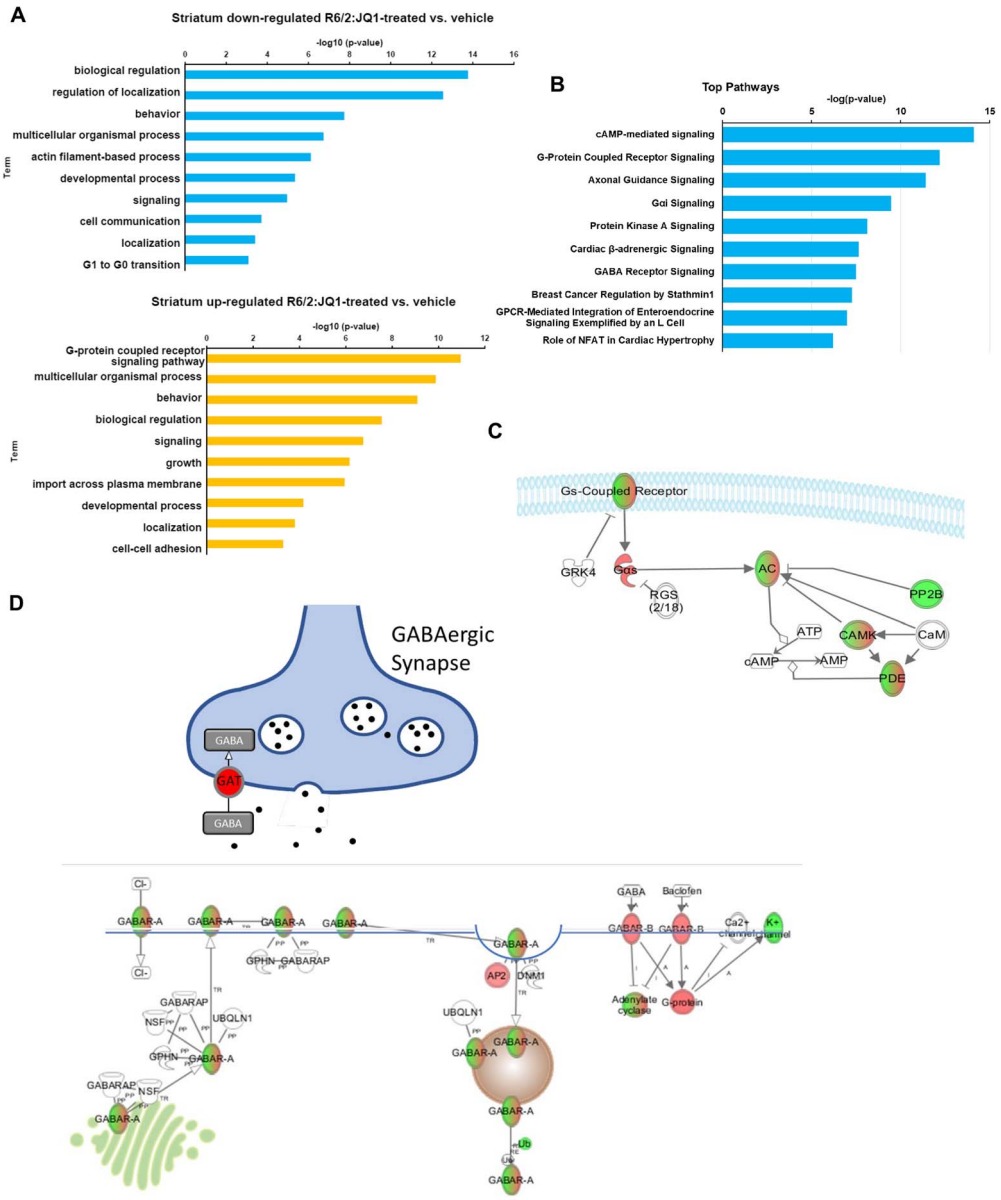

Figure 10. GO and pathway analysis of genes dysregulated by JQ1 treatment in striatum of R6/2 mice. (**A**) GO analysis of JQ1-treated R6/2 striatum. (**B**) IPA pathway analysis of JQ1-treated R6/2 striatum showing enrichment of neuronal related pathways in R6/2 JQ1-treated striatum. Striatal R6/2 JQ1-treated versus vehicle DEGs also have an overrepresentation of (**C**) phosphodiesterases and (**D**) GABA receptors.

found to affect transcription of synaptic proteins and receptors in neurons in wild-type mice (37). Therefore, the deleterious effects of JQ1 in R6/2 mice could reflect an extra vulnerability of HD brains to selective dysregulation of synaptic-activity-induced gene expression.

When we evaluated the NT mice, we found JQ-1 treatment in cortex displayed a significant up-regulation of genes involved in translational regulation, particularly eIF3, and in ETC genes, which would be necessary to provide energy for increased translational activity. This increase in gene transcription for bioenergetics and translation could relate to the enhanced activity in motor ability in NT mice with drug treatment. Dysregulation of mRNA translation has recently been implicated in neurodegeneration through mutations in translation machinery or from inappropriate activation of integrated stress responses. Further, subtle disruptions in translational regulation can have dramatic consequences for survival of neurons (43). The lack of a similar up-regulation of genes involved in translational regulation by JQ1 in R6/2 mice could therefore impact factors that could be rate limiting through translational regulation at synapses and affect synaptic activity. Additional research will be needed to test these hypotheses.

Materials and Methods

JQ1 Treatment of R6/2 Mice

All animal procedures were performed in accordance with National Institutes of Health and University of California guidelines. R6/2 transgenic (~120 +/−5 CAG repeat) mice and their NT littermates were obtained from the Jackson Laboratory. JQ1, bromodomain inhibitor (for BRD2, 3, 4 and T) chemical

name: tert-butyl 2-((6S)-4-(4-chlorophenyl)-2,3,9-trimethyl-6H-thieno[3,2-f][1,2,4]triazolo[4,3-a][1,4]diazepin-6-yl) acetate was provided by the James Bradner Laboratory at Dana-Farber Cancer Institute. JQ1 was prepared daily by thawing a concentrated stock in DMSO prepared at a concentration of 50 mg/ml, adding 10% vehicle [(2-hydroxypropyl)-β-cyclodextrin in sterile milliQ-purified H_2O] dropwise to allow a dosing volume of 10ul/g of body weight at a final dose of 50 mg/kg. R6/2 and age-matched NT male mice (n = 10/group) were obtained at 5 weeks of age and dosed by daily intraperitoneal injection after a brief acclimation period. Mice were tested in behavior tasks each week thereafter and then sacrificed at 11 weeks of age. All mice were housed on a 12-h light/dark schedule with ad libitum access to food and water, mice were weighed daily. *Behavioral Assessment:* Mice were assigned to groups in a semi-randomized manner. Behavioral tests were performed at 6, 7, 8, 9 or 10 weeks of age depending on the task. Researchers were blind to which mice had been injected during experiment testing and data collection. To minimize experimenter variability a single investigator conducted each behavioral test. Rotarod, pole test and grip strength were performed as described (30). Assessment of differences in outcome were based upon previous experience and published results (44,45) for HD models and applying power analysis [G Power (http://www.psycho.uni-duesseldorf.de/abteilungen/aap/gpower3/)] led us to a minimum of 10 for behavior and 4 for biochemical analysis. At the end of the study, mice were sacrificed and three from each group were perfused with PBS and whole brains were drop fixed into paraformaldehyde for immunohistochemistry. The other seven mice were sacrificed and striatum, cortex and cerebellum brain sections from each hemisphere were collected by microdissection and snap frozen for analysis. Tissues from four mice for each group were selected and one hemisphere of cortex and one hemisphere of striatum were sent to MIT for ChIP-Seq analysis. The corresponding hemispheres were analyzed for RNA-Seq at UCI.

Soluble/insoluble fractionation

Striatal tissue was processed as described previously and western blot analysis performed (30). Antibody: Anti-HTT (Millipore Cat# MAB5492 RRID:AB 347723). Detection was performed using the Li-Cor Odyssey Clx system and REVERT total protein stain for normalization as per manufacturers protocols (LiCor, Lincoln, Nebraska). Quantification of bands performed using software from NIH program ImageJ and densitometry application.

mRNA sequencing, mapping and statistical analysis

RNA was extracted using Trizol and Qiagen RNeasy mini kits for 28 samples (16 cortical and 12 striatal) of JQ1-treated and vehicle R6/2 and NT mouse brains. Four cortices and three striata for each group (NT and R6/2, treated and vehicle) were evaluated. RNAs were checked for quality using an Agilent 2100 Bioanalyzer. All samples had RNA integrity (RIN) values above 9.4. Each sample then underwent library prep using the non-stranded Truseq mRNA PolyA+ v2 lib prep kit with 1ug of RNA and ERCC Exfold spike-ins were added. mRNA sequencing was conducted across four lanes on the HiSeq 2500 yielding ~800 M paired end, 100 bp reads. These reads were first QC analyzed using FASTQC (v. 0.11.2), then trimmed using Trimmomatic (v.0.35) with Illumina TruSeq adapter sequences, PHRED quality score 15 and minimum length 20 bases. The trimmed reads were then aligned to mouse mm10 reference genome with transcriptome annotation and post-processed using Tophat2 (v.2.1.0), Bowtie2 (v.2.2.3) and Samtools(v.1.3). Gene level expression was then quantified both with FPKM (fragment per kilobase per million mapped reads) using Cufflinks (v. 2.1.1) and with raw counts using HTSeq (v.0.6.1p1.). Differential expression analysis was done using DESeq2, and a list of differentially expressed genes was generated using a FDR of 10% for six statistical comparisons: striatum: R6/2 vehicle versus NT untreated, R6/2 vehicle versus treated and CTRL vehicle versus treated; cortex: R6/2 vehicle versus NT untreated, R6/2 vehicle versus treated and CTRL vehicle versus treated. GOrilla (33) and IPA (Qiagen) were used for GO enrichment analysis and pathway analysis.

ChIP-seq, mapping and statistical analysis

Cortex samples (a single mouse per condition) were prepared using MAgnify™ ChIP kit (ThermoFisher) according to manufacturer's instructions, using the following antibodies: H3K4me3 (Millipore, 07–473), H3K27ac (Abcam, ab4729) and rabbit IgG (Santa Cruz, sc-2027). Striatum samples (three mice per condition) were processed using N-ChIP protocol, which is better optimized for very small tissue samples such as the striatum. Lysis buffer (50 mM Tris-HCl pH 8, 150 mM NaCl, 5 mM $CaCl_2$, 1% Triton® X-100, 0.1% Na-deoxycholate, 5 mM Na Butyrate and Proteinase inhibitors) was added to the pulverized tissues and the samples were transferred through 40 µ cell strainer and incubated on ice for 20 min. The lysates were digested with MNase (NEB) for 10 min at 37°C and the reaction was terminated by addition of 10 mM of EDTA. The samples were incubated with the antibodies overnight at 4°C. On the next day, 25 ul protein G beads (Dynabeads) were added to each sample and further incubated for 2 hr at 4°C. The samples were briefly washed seven times; two washes with RIPA buffer (10 mM Tris-HCl pH 8,1 mM EDTA, 140 mM NaCl, 1% Triton® X-100, 0.1% Na-Deoxycholate, 0.1% SDS), two washes with high salt RIPA buffer (10 mM Tris-HCl pH 8,1 mM EDTA, 360 mM NaCl, 1% Triton® X-100, 0.1% Na-Deoxycholate, 0.1% SDS), two washes with LiCl buffer (10 mM Tris-HCl pH 8, 1 mM EDTA, 250 mM LiCl, 0.5% Igepal, 0.5% Na-Deoxycholate) and a final wash with TE. The DNA was eluted with Elution Buffer (10 mM Tris-HCl pH 8, 5 mM EDTA, 300 mM NaCl, 0.1% SDS, 2 U Proteinase K) for 1 hr at 62°C, and the DNA was purified using Agencourt AMPure beads (Beckman Coulter). A total of 10 ng of DNA was used for libraries preparations using NEBNext® Ultra™ II DNA Library Prep Kit for Illumina® (NEB). The libraries' quality and concentration were tested using a Fragment Analyzer™ instrument (Advanced Analytical) and by a qPCR-based method (KAPA Library Quantification Kit for Illumina Sequencing Platforms). The samples were sequenced with the Illumina HiSeq 2000 platform (MIT BioMicro center).

Reads were aligned to the mm10 genome with Bowtie2 (Langmead and Salzberg 2012). A high number of reads (77–99%) were successfully aligned in all cases except for NT vehicle H3K4me3 in cortex, where it is likely a PCR error led to a high number of repetitive reads. However, aligning only the unique reads to the genome led to 54% alignment rate, meaning over 11 million aligned unique reads were carried on to further analysis.

ChIP-seq peaks were identified for all samples by comparing to an IgG control in the striatum. The peak-calling software package SICER v1.1 (46) was chosen for this analysis because of its use in finding the extremely wide peaks that are common in histone mark ChIP-seq experiments. For H3K4me3 and H3K27ac, over 50% of reads fell under called peaks. For the cortex samples, where only a single mouse was used for ChIP-seq, the differential peak calling software MAnorm (47) was then used to find peaks that were significantly different between pairs

of samples. For H3K4me3 and H3K27ac in the striatum, ChIP-seq was performed in three individual mice. For these cases, MAnorm was used to confirm high agreement between replicates (>96% of peaks called as 'unbiased', or common between replicates, in every case). Differential peaks between conditions were called using DiffBind (48) with the DESeq2 algorithm (49). Genes were assigned to peaks if their TSS fell within 10 kb of the peak boundaries, and then lists of nearby peaks were submitted to Enrichr (Chen et al. 2013) and checked for Gene Ontology Biological Process enrichment.

Supplementary Material

Supplementary Material is available at *HMG* online.

Funding

This work was supported primarily by the CHDI Foundation (to L.M.T. and E.F.). Additional support was provided by National Institutes of Health (NS089076 to L.M.T. and E.F., NS090390 to L.M.T.), NeuroLINCS center (U54 NS091046 to L.M.T. and E.F.), NIH/NIGMS Biotechnology Training Program T32 (GM008334 to A.J. K.) and Ruth L. Kirschstein Predoctoral (NRSA 1F31NS090859-01 to R.G.L.). This work was made possible, in part, through access to the Genomic High Throughput Facility Shared Resource of the Cancer Center Support Grant (CA-62203) at the University of California, Irvine. Support also included computing resources from National Science Foundation (grant DB1-0821391) and sequencing support from National Institutes of Health (grant P30-ES002109).

Acknowledgments

We thank James Bradner for providing JQ1 for the study.

Conflict of Interest statement. None declared.

References

1. The Huntington's Disease Collaborative Research Group (1993) A novel gene containing a trinucleotide repeat that is expanded and unstable on Huntington's disease chromosomes. *Cell*, **72**, 971–983.
2. Ross, C.A. and Tabrizi, S.J. (2011) Huntington's disease: from molecular pathogenesis to clinical treatment. *Lancet. Neurol.*, **10**, 83–98.
3. Valor, L.M. (2015) Transcription, epigenetics and ameliorative strategies in Huntington's disease: a genome-wide perspective. *Mol. Neurobiol.*, **51**, 406–423.
4. Achour, M., Le, S., Keime, C., Parmentier, F., Lejeune, F.X., Boutillier, A.L., Neri, C., Davidson, I. and Merienne, K. (2015) Neuronal identity genes regulated by super-enhancers are preferentially down-regulated in the striatum of Huntington's disease mice. *Hum. Mol. Genet.*, **24**, 3481–3496.
5. Consortium, H.D.I. (2017) Developmental alterations in Huntington's disease neural cells and pharmacological rescue in cells and mice. *Nat. Neurosci.*, **20**, 648–660.
6. Le, S., Keime, C., Anthony, A., Lotz, C., De Longprez, L., Brouillet, E., Cassel, J.C., Boutillier, A.L. and Merienne, K. (2017) Altered enhancer transcription underlies Huntington's disease striatal transcriptional signature. *Sci. Rep.*, **7**, 42875.
7. Vashishtha, M., Ng, C.W., Yildirim, F., Gipson, T.A., Kratter, I.H., Bodai, L., Song, W., Lau, A., Labadorf, A., Vogel-Ciernia, A. *et al.* (2013) Targeting H3K4 trimethylation in Huntington disease. *Proc. Natl. Acad. Sci. U. S. A*, **110**, E3027–E3036.
8. Hockly, E., Richon, V.M., Woodman, B., Smith, D.L., Zhou, X., Rosa, E., Sathasivam, K., Ghazi-Noori, S., Mahal, A., Lowden, P.A. *et al.* (2003) Suberoylanilide hydroxamic acid, a histone deacetylase inhibitor, ameliorates motor deficits in a mouse model of Huntington's disease. *Proc. Natl. Acad. Sci. USA.*
9. Steffan, J.S., Bodai, L., Pallos, J., Poelman, M., McCampbell, A., Apostol, B.L., Kazantsev, A., Schmidt, E., Zhu, Y.Z., Greenwald, M. *et al.* (2001) Histone deacetylase inhibitors arrest polyglutamine-dependent neurodegeneration in drosophila. *Nature*, **413**, 739–743.
10. Delmore, J.E., Issa, G.C., Lemieux, M.E., Rahl, P.B., Shi, J., Jacobs, H.M., Kastritis, E., Gilpatrick, T., Paranal, R.M., Qi, J. *et al.* (2011) BET bromodomain inhibition as a therapeutic strategy to target c-Myc. *Cell*, **146**, 904–917.
11. Filippakopoulos, P., Qi, J., Picaud, S., Shen, Y., Smith, W.B., Fedorov, O., Morse, E.M., Keates, T., Hickman, T.T., Felletar, I. *et al.* (2010) Selective inhibition of BET bromodomains. *Nature*, **468**, 1067–1073.
12. Albrecht, B.K., Gehling, V.S., Hewitt, M.C., Vaswani, R.G., Cote, A., Leblanc, Y., Nasveschuk, C.G., Bellon, S., Bergeron, L., Campbell, R. *et al.* (2016) Identification of a benzoisoxazoloazepine inhibitor (CPI-0610) of the bromodomain and extra-terminal (BET) family as a candidate for human clinical trials. *J. Med. Chem.*, **59**, 1330–1339.
13. Muller, S., Filippakopoulos, P. and Knapp, S. (2011) Bromodomains as therapeutic targets. *Expert Rev. Mol. Med.*, **13**, e29.
14. Qi, J. (2014) Bromodomain and extraterminal domain inhibitors (BETi) for cancer therapy: chemical modulation of chromatin structure. *Cold Spring Harb. Perspect. Biol.*, **6**, a018663.
15. Cheng, Z., Gong, Y., Ma, Y., Lu, K., Lu, X., Pierce, L.A., Thompson, R.C., Muller, S., Knapp, S. and Wang, J. (2013) Inhibition of BET bromodomain targets in genetically diverse glioblastoma. *Clin. Cancer Res.*, **19**, 1748–1759.
16. Magistri, M., Velmeshev, D., Makhmutova, M., Patel, P., Sartor, G.C., Volmar, C.H., Wahlestedt, C. and Faghihi, M.A. (2016) The BET-bromodomain inhibitor JQ1 reduces inflammation and tau phosphorylation at Ser396 in the brain of the 3xTg model of Alzheimer's disease. *Curr. Alzheimer Res.*, **13**, 985–995.
17. Wang, H., Huang, W., Liang, M., Shi, Y., Zhang, C., Li, Q., Liu, M., Shou, Y., Yin, H., Zhu, X. *et al.* (2018) (+)-JQ1 attenuated LPS-induced microglial inflammation via MAPK/NFkappaB signaling. *Cell Biosci.*, **8**, 60.
18. Loven, J., Hoke, H.A., Lin, C.Y., Lau, A., Orlando, D.A., Vakoc, C.R., Bradner, J.E., Lee, T.I. and Young, R.A. (2013) Selective inhibition of tumor oncogenes by disruption of super-enhancers. *Cell*, **153**, 320–334.
19. Sengupta, D., Kannan, A., Kern, M., Moreno, M.A., Vural, E., van Stack, B.,J., Suen, J.Y., Tackett, A.J. and Gao, L. (2015) Disruption of BRD4 at H3K27Ac-enriched enhancer region correlates with decreased c-Myc expression in Merkel cell carcinoma. *Epigenetics*, **10**, 460–466.
20. Shi, X., Liu, C., Liu, B., Chen, J., Wu, X. and Gong, W. (2018) JQ1: a novel potential therapeutic target. *Pharmazie*, **73**, 491–493.
21. Li, J., Zhao, L., Urabe, G., Fu, Y. and Guo, L.W. (2017) Epigenetic intervention with a BET inhibitor ameliorates acute retinal ganglion cell death in mice. *Mol. Vis.*, **23**, 149–159.
22. Jung, K.H., Das, A., Chai, J.C., Kim, S.H., Morya, N., Park, K.S., Lee, Y.S. and Chai, Y.G. (2015) RNA sequencing reveals distinct mechanisms underlying BET inhibitor JQ1-mediated

modulation of the LPS-induced activation of BV-2 microglial cells. *J Neuroinflammation*, **12**, 36.
23. Santos-Rosa, H., Schneider, R., Bannister, A.J., Sherriff, J., Bernstein, B.E., Emre, N.C., Schreiber, S.L., Mellor, J. and Kouzarides, T. (2002) Active genes are tri-methylated at K4 of histone H3. *Nature*, **419**, 407–411.
24. Dong, X., Tsuji, J., Labadorf, A., Roussos, P., Chen, J.F., Myers, R.H., Akbarian, S. and Weng, Z. (2015) The role of H3K4me3 in transcriptional regulation is altered in Huntington's disease. *PloS one*, **10**, e0144398.
25. Creyghton, M.P., Cheng, A.W., Welstead, G.G., Kooistra, T., Carey, B.W., Steine, E.J., Hanna, J., Lodato, M.A., Frampton, G.M., Sharp, P.A. *et al*. (2010) Histone H3K27ac separates active from poised enhancers and predicts developmental state. *Proc. Natl. Acad. Sci. USA*, **107**, 21931–21936.
26. Heintzman, N.D., Hon, G.C., Hawkins, R.D., Kheradpour, P., Stark, A., Harp, L.F., Ye, Z., Lee, L.K., Stuart, R.K., Ching, C.W. *et al*. (2009) Histone modifications at human enhancers reflect global cell-type-specific gene expression. *Nature*, **459**, 108–112.
27. Zhang, W., Prakash, C., Sum, C., Gong, Y., Li, Y., Kwok, J.J., Thiessen, N., Pettersson, S., Jones, S.J., Knapp, S., Yang, H. and Chin, K.C. (2012) Bromodomain-containing protein 4 (BRD4) regulates RNA polymerase II serine 2 phosphorylation in human CD4+ T cells. *J. Biol. Chem.*, **287**, 43137–43155.
28. Mangiarini, L., Sathasivam, K., Seller, M., Cozens, B., Harper, A., Hetherington, C., Lawton, M., Trottier, Y., Lehrach, H., Davies, S.W. and Bates, G.P. (1996) Exon 1 of the HD gene with an expanded CAG repeat is sufficient to cause a progressive neurological phenotype in transgenic mice. *Cell*, **87**, 493–506.
29. Hodges, A., Strand, A.D., Aragaki, A.K., Kuhn, A., Sengstag, T., Hughes, G., Elliston, L.A., Hartog, C., Goldstein, D.R., Thu, D. *et al*. (2006) Regional and cellular gene expression changes in human Huntington's disease brain. *Hum. Mol. Genet.*, **15**, 965–977.
30. Ochaba, J., Monteys, A.M., O'Rourke, J.G., Reidling, J.C., Steffan, J.S., Davidson, B.L. and Thompson, L.M. (2016) PIAS1 regulates mutant Huntingtin accumulation and Huntington's disease-associated phenotypes in vivo. *Neuron*, **90**, 507–520.
31. Reidling, J.C., Relano-Gines, A., Holley, S.M., Ochaba, J., Moore, C., Fury, B., Lau, A., Tran, A.H., Yeung, S., Salamati, D. *et al*. (2018) Human neural stem cell transplantation rescues functional deficits in R6/2 and Q140 Huntington's disease mice. *Stem Cell Reports*, **10**, 58–72.
32. O'Rourke, J.G., Gareau, J.R., Ochaba, J., Song, W., Rasko, T., Reverter, D., Lee, J., Monteys, A.M., Pallos, J., Mee, L. *et al*. (2013) SUMO-2 and PIAS1 modulate insoluble mutant huntingtin protein accumulation. *Cell Reports*, **4**, 362–375.
33. Eden, E., Navon, R., Steinfeld, I., Lipson, D. and Yakhini, Z. (2009) GOrilla: a tool for discovery and visualization of enriched GO terms in ranked gene lists. *BMC Bioinformatics*, **10**, 48.
34. Xu, X., Wells, A.B., O'Brien, D.R., Nehorai, A. and Dougherty, J.D. (2014) Cell type-specific expression analysis to identify putative cellular mechanisms for neurogenetic disorders. *J Neurosci.*, **34**, 1420–1431.
35. Kramer, A., Green, J., van Pollard, J.,J. and Tugendreich, S. (2014) Causal analysis approaches in ingenuity pathway analysis. *Bioinformatics*, **30**, 523–530.
36. Consortium, T.H.I. (2012) Induced pluripotent stem cells from patients with Huntington's disease show CAG-repeat-expansion-associated phenotypes. *Cell Stem Cell*, **11**, 264–278.
37. Korb, E., Herre, M., Zucker-Scharff, I., Darnell, R.B. and Allis, C.D. (2015) BET protein Brd4 activates transcription in neurons and BET inhibitor Jq1 blocks memory in mice. *Nat Neurosci.*, **18**, 1464–1473.
38. Winter, G.E., Mayer, A., Buckley, D.L., Erb, M.A., Roderick, J.E., Vittori, S., Reyes, J.M., di Iulio, J., Souza, A., Ott, C.J. *et al*. (2017) BET Bromodomain proteins function as master transcription elongation factors independent of CDK9 recruitment. *Mol. Cell*, **67**, **e19**, 5–18.
39. Rathert, P., Roth, M., Neumann, T., Muerdter, F., Roe, J.S., Muhar, M., Deswal, S., Cerny-Reiterer, S., Peter, B., Jude, J. *et al*. (2015) Transcriptional plasticity promotes primary and acquired resistance to BET inhibition. *Nature*, **525**, 543–547.
40. Shu, S., Lin, C.Y., He, H.H., Witwicki, R.M., Tabassum, D.P., Roberts, J.M., Janiszewska, M., Huh, S.J., Liang, Y., Ryan, J. *et al*. (2016) Response and resistance to BET bromodomain inhibitors in triple-negative breast cancer. *Nature*, **529**, 413–417.
41. Kanno, T., Kanno, Y., LeRoy, G., Campos, E., Sun, H.W., Brooks, S.R., Vahedi, G., Heightman, T.D., Garcia, B.A., Reinberg, D. *et al*. (2014) BRD4 assists elongation of both coding and enhancer RNAs by interacting with acetylated histones. *Nat. Struct. Mol. Biol.*, **21**, 1047–1057.
42. Najafova, Z., Tirado-Magallanes, R., Subramaniam, M., Hossan, T., Schmidt, G., Nagarajan, S., Baumgart, S.J., Mishra, V.K., Bedi, U., Hesse, E. *et al*. (2017) BRD4 localization to lineage-specific enhancers is associated with a distinct transcription factor repertoire. *Nucleic Acids Res.*, **45**, 127–141.
43. Kapur, M., Monaghan, C.E. and Ackerman, S.L. (2017) Regulation of mRNA translation in neurons-a matter of life and death. *Neuron*, **96**, 616–637.
44. Hickey, M.A. and Chesselet, M.F. (2003) The use of transgenic and knock-in mice to study Huntington's disease. *Cytogenet Genome Res.*, **100**, 276–286.
45. Hockly, E., Woodman, B., Mahal, A., Lewis, C.M. and Bates, G. (2003) Standardization and statistical approaches to therapeutic trials in the R6/2 mouse. *Brain. Res. Bull.*, **61**, 469–479.
46. Zang, C., Schones, D.E., Zeng, C., Cui, K., Zhao, K. and Peng, W. (2009) A clustering approach for identification of enriched domains from histone modification ChIP-Seq data. *Bioinformatics*, **25**, 1952–1958.
47. Shao, Z., Zhang, Y., Yuan, G.C., Orkin, S.H. and Waxman, D.J. (2012) MAnorm: a robust model for quantitative comparison of ChIP-Seq data sets. *Genome Biol.*, **13**, R16.
48. Ross-Innes, C.S., Stark, R., Teschendorff, A.E., Holmes, K.A., Ali, H.R., Dunning, M.J., Brown, G.D., Gojis, O., Ellis, I.O., Green, A.R. *et al*. (2012) Differential oestrogen receptor binding is associated with clinical outcome in breast cancer. *Nature*, **481**, 389–393.
49. Love, M.I., Huber, W. and Anders, S. (2014) Moderated estimation of fold change and dispersion for RNA-seq data with DESeq2. *Genome Biol.*, **15**, 550.
50. Thorvaldsdottir, H., Robinson, J.T. and Mesirov, J.P. (2013) Integrative genomics viewer (IGV): high-performance genomics data visualization and exploration. *Brief Bioinform*, **14**, 178–192.
51. Khan, A. and Zhang, X. (2016) dbSUPER: a database of super-enhancers in mouse and human genome. *Nucleic Acids Res.*, **44**, D164–D171.